



Article

A Circulation Weather Type Analysis of Urban Effects on Daily Thermal Range for Milan (Italy)

Giuseppe Colangelo ¹, Giovanni Sanesi ^{1,*}, Luigi Mariani ², Simone G. Parisi ³ and Gabriele Cola ²
¹ Department of Agricultural and Environmental Sciences, University of Bari Aldo Moro, 70121 Bari, Italy

² Department of Agricultural and Environmental Sciences—Production, Landscape, Agroenergy, University of Milan, 20122 Milan, Italy

³ Abaco SpA, 46100 Mantova, Italy

* Correspondence: giovannisanesi@uniba.it; Tel.: +39-0805443023

Abstract: We present a first attempt to analyse the effect of a large urban park (Parco Nord Milano—PNM) on the Urban Heat Island (UHI) of the city area of Milan. Specifically, analysis of the effect of three cyclonic and three anticyclonic circulation weather types (CWTs) on the frequency distribution of the daily thermal range (DTR) of five weather stations in Milan shows the stabilizing effect of the city on the DTR when compared with suburban and rural areas, generating a modal class of 4 °C in winter and 9 °C in summer. In parallel, a temperature transect of the urban park Parco Nord Milano was performed by bicycle during a day of anticyclonic summer weather in order to understand the effect of the park on the UHI. This investigation highlighted the homogenization effect on temperatures induced by the thermal turbulence triggered by intense sunshine.

Keywords: weather types; urban heat island; urban temperature studies



Citation: Colangelo, G.; Sanesi, G.; Mariani, L.; Parisi, S.G.; Cola, G. A Circulation Weather Type Analysis of Urban Effects on Daily Thermal Range for Milan (Italy). *Atmosphere* **2022**, *13*, 1529. <https://doi.org/10.3390/atmos13091529>

Academic Editor: Chuan Yao Lin

Received: 9 August 2022

Accepted: 13 September 2022

Published: 19 September 2022

Publisher's Note: MDPI stays neutral with regard to jurisdictional claims in published maps and institutional affiliations.



Copyright: © 2022 by the authors. Licensee MDPI, Basel, Switzerland. This article is an open access article distributed under the terms and conditions of the Creative Commons Attribution (CC BY) license (<https://creativecommons.org/licenses/by/4.0/>).

1. Introduction

Urban Heat Island (UHI) is an expression first coined in the 1940s to refer to the atmospheric warmth of a city compared to its countryside. Heat islands occur in almost all urban areas, large or small, as well as in warm and cold climates. The traditionally described heat island is measured at standard screen height (1.50–2.00 m above ground), below the city's mean roof height in a part of the boundary layer called the urban canopy layer [1], which is analogous with the rural boundary layer, i.e., the atmospheric layer below the top of the vegetation cover.

DTR is among the main indicators of the presence and strength of a UHI, as stated by Varquez and Kanda [2], who examined the relationship between global UHI trends and geophysical and anthropogenic factors.

The main causes of the UHI relate to structural and land cover differences between urban and rural areas, which affect the surface energy balance (SEB) [3–5]. Cities comprise buildings extending above ground level, and they are dry and impervious, with construction materials extending across natural soils and vegetation.

Surface energy balance is the microscale determinant of the climate of a given site by means of the fluxes of net radiation, as well as sensible and latent heat. Even if the abovementioned fluxes taking place in the boundary layer can be considered microscale phenomena [5], they are influenced by larger scales, both horizontally (meso and macro scales) and vertically (planetary boundary layer and free atmosphere). In this work, we consider the base of circulation weather types (CWTs) [6].

The taxonomical approach to CWT has a long history, including, for example, the 10-type classification for Italy proposed by Filippo Eredia based on sea level pressure (1941); the Grosswetterlage model proposed by Hess and Brezowsky (1952) for Europe and the northeast Atlantic, with a primary focus on central Europe; the Lamb classification for the British Isles (1972); and more recently, the MeteoSwiss classification [7]. The oldest

classifications were based on surface pressure fields, whereas today, classifications often rely on upper air patterns.

In terms of methodology, CWT taxonomy can be defined with cluster analysis, principal component analysis and empirical orthogonal function analysis, yielding sets of basic spatial patterns representing the most dominant modes of circulation variability. However, the primary resulting patterns always tend to be large-scale smooth structures, which do not intrinsically capture real synoptic characteristics. Furthermore, some synoptic types, which are infrequent but relevant for operational purposes, are not detected.

Given these problems, the subjective preselection of a set of basis patterns for classification based on experience in synoptic and mesoscale analysis, is still useful and meaningful for users, with an intuitive naming convention related to the human experience of weather phenomena [8].

In this regard, it is important to highlight the automation of pattern recognition on the basis of well-known taxonomical systems, as in the case of the Jenkinson and Collinson method referring to the Lamb classification [9], the James method [8] referring to the Gross-wetterlage system and the panoply of methods based on trained neural networks [10,11].

Circulation weather types have been extensively used to study relationships between atmospheric circulation at macro or meso scales, as well as several small-scale meteorological features [12], such as precipitation [13–15], tornadoes [16,17], air quality [18,19], and urban microclimate [20–27].

In this work, we refer to the urban area of Milan, which is located in the basin of the Po River (the main basin in Italy), opening to the East toward the Adriatic Sea and surrounded by the Alps on the northern and western sides (with an average height of about 3000 m a.s.l.) and by the Apennines on the southern side (average height of about 800 m a.s.l.). In this way, the mass of air inside the valley is partially isolated from the external environment and undergoes peculiar effects, such as:

- The advection of continental air masses from the east due to blocking anticyclones centred in Poland and the Baltic area;
- Strong thunderstorm activity during summer triggered by the advection of Arctic and Polar maritime air masses in the middle troposphere (more than 3000 m a.s.l.). In the Po valley, such situations are enhanced by the remarkable stability of air masses in low layers caused by the action of dynamic anticyclones, leading to the accumulation of humidity in the planetary boundary layer (PBL);
- Blocking anticyclones present in all seasons with accumulation of pollutants in the PBL and relevant presence of fog from fall to spring.

The effect of the Urban Heat Island (UHI) on the majority of meteorological variables in the urban boundary layer has been widely studied in recent decades [4,28,29], showing, for example, that:

- The UHI can be described continuous measurements by weather stations and discontinuous measurements by remote sensing technologies (satellite images and drones) or field monitoring campaigns;
- UHI is a microscale effect superimposed to meso and macroscale weather phenomena. Specifically, the UHI climate is strongly modulated by macroclimatic features, described, for example, by Koeppen classification [30]: mean and extreme features of UHI for oceanic climates (Cf) differ from the UHI in Mediterranean climates (Cs climates);
- Different types of tree canopies (in terms of physical and biological features) affect UHI, impacting the surface energy balance (SEB), e.g., latent heat fluxes from vegetation and water bodies, shadow effects, sky view factor and albedo.

The aim of this work is to analyse how CWT affects the Urban Heat Island of a metropolitan city by analysing 13-year-long time series gathered by five weather stations representing different boundary layer types, from fully rural to fully urban, with transitional patterns affected by the large urban park Parco Nord Milano [31,32]. Additionally, we

performed 24 h monitoring of temperature across a city transect in order to detect the effects of a large green urban area (Parco Nord Milano) on UHI during an anticyclonic CWT.

2. Materials and Methods

2.1. Circulation Weather Type Taxonomy

The taxonomic scheme of the CWT used for this work is refers to topographies of the 850 hPa geopotential level.

The 850 hPa level is usually just above the boundary layer, and for an area with a complex orography, such as northern Italy, this level highlights the effects on circulation of the Alps, the average altitude of which is 3000 m a.s.l.

Synoptic CWTs at 850 hPa exert a significant effect on the DTR in different ways. For example, they (i) act on the meteorological variables at ground level (cloud coverage, precipitation, relative humidity, wind, etc.), which influence the surface radiative and energy balance; (ii) give rise to advective effects with horizontal transport of hot/cold air; and (iii) trigger convective and catabatic effects with heating and cooling of surface air masses.

Seventeen weather types are described in Table 1, inspired by the taxonomic scheme defined by Borghi and Giuliani [33]. Daily pattern recognition for the 1 January 2002 to 31 December 2015. 1 January 2002 period was performed in a subjective way by analysing the weather maps produced by NOAA (2022) [34] for the reference area defined in the coordinate range of 30° N to 70° N latitude and −40° E to 40° E longitude.

Table 1. CWT classification (C = cyclonic, Ac = anticyclonic, I = intermediate).

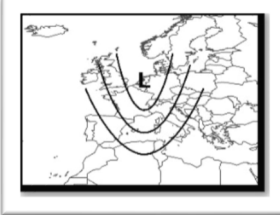
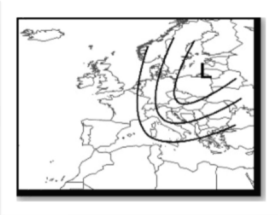
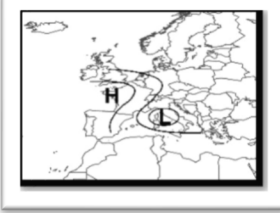
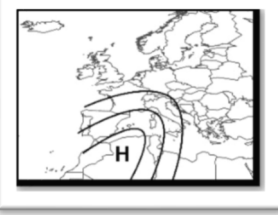
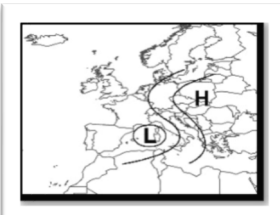
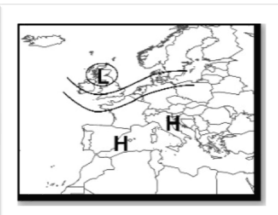
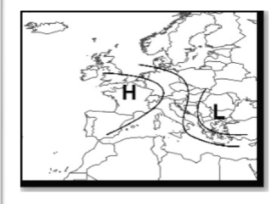
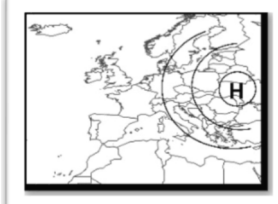
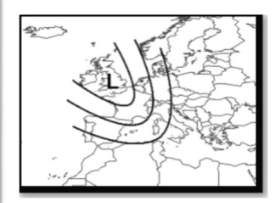
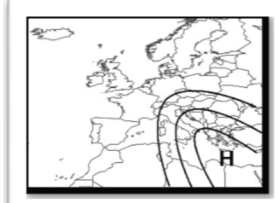
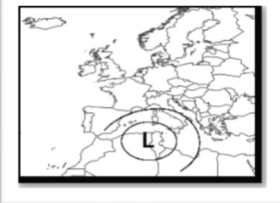
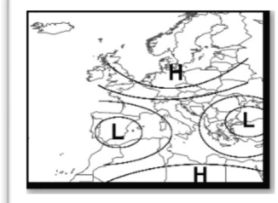
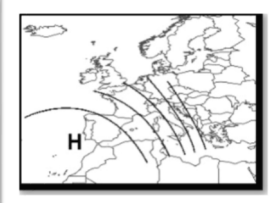
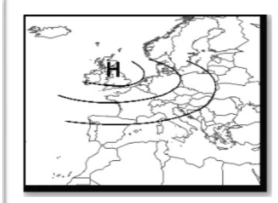

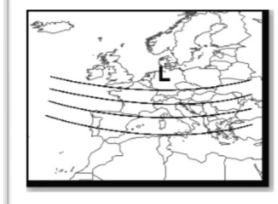
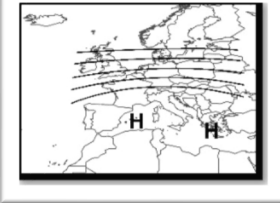
Description		Description	
1—Northern trough (C)		10—North-easterly trough (C)	
trough with North or slightly tilted axis over the western Mediterranean		trough with axis from North-East	
2—Genoa low (C)		11—South-westerly ridge (Ac)	
inverted S-shaped pattern with (i) Mediterranean low on the Ligurian – Upper Tyrrhenian Sea and (ii) anticyclonic ridge with axis from the Atlantic Ocean towards the northern Alpine side		anticyclonic ridge with axis from South-West	
3—Western Mediterranean low (C)		12—Lowering anticyclone (Ac)	
S-shaped pattern with (i) low on the Central-Western Mediterranean and (ii) anticyclonic ridge with axis from Eastern Europe towards the Northern Alpine slope		over the Mediterranean a flat anticyclonic field is lowering due to a trough approaching from North-West	

Table 1. Cont.

Description		Description	
4—Balkans low (I)		13—Russian anticyclone (Ac)	
inverted S-shaped pattern with (i) low over the Balkans and (ii) anticyclonic ridge with axis from the Atlantic Ocean towards the Alps		anticyclone over Central-East Europe with easterly flow	
5—Northwesterly Trough (C)		14—Southeastern Anticyclonic ridge (Ac) t	
trough with axis from North-West		anticyclonic ridge with axis from southeast	
6—North African low (C)		15—Easterly flow (I)	
low over North-West Africa—Southern Mediterranean		belt of Mediterranean lows with easterly flow	
7—Foehn (I)		16—Anticyclonic ridge from Nord-west (Ac)	
fast North-Western air masses flow on the eastern side of a subtropical anticyclonic ridge with axis from the south on the nearby Atlantic		anticyclonic ridge with axis from North-West	
8—African anticyclone e (Ac)		17—Mediterranean westerlies (I)	
anticyclonic ridge with axis from South		westerlies over the Mediterranean	
9—African ridge (Ac)			
zonal flow over Central Europe. Over the Mediterranean flat anticyclonic field			

During anticyclonic weather types, with an average of 116 days of occurrence per year, the boundary layer is well-structured, with thermal inversion during night, which is dissipated during daytime by convective patterns induced by solar heating of surfaces [22]. Dynamic anticyclones affecting the Po valley can be subdivided into blocking anticy-

clones [35], which persist for a relevant number of days (3 to 12 days or more), and mobile anticyclones, which quickly cross the area and are often followed by Atlantic disturbances.

The boundary layer during cyclonic weather types is disrupted by circulation patterns unsuitable for the persistence of well-structured layers.

Air temperature (measured at 1.8 m above ground level in the urban canopy layer) was obtained from 5 weather stations of the Meteorological Service of ARPA Lombardia (<https://www.arpalombardia.it/Pages/Meteorologia/Richiesta-dati-misurati.aspx> (accessed on 15 June 2022) (Figure 1).

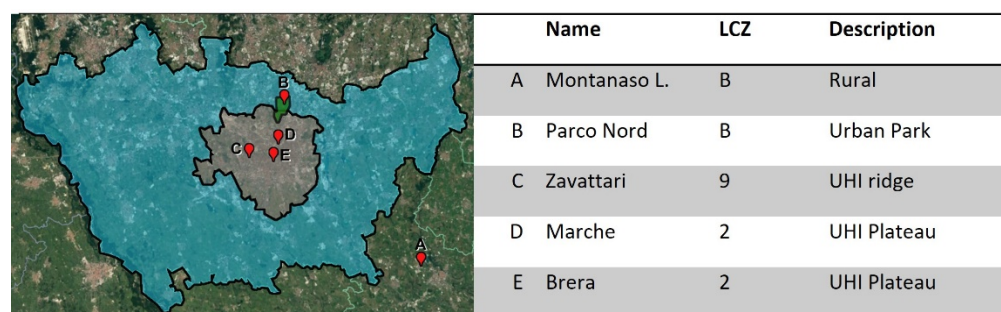


Figure 1. Position of the five weather stations. Blue area = metropolitan city; grey area = Milan municipality; green area = Parco Nord.

The five sites were chosen to represent different sectors of the Urban Heat Island of Milano and were classified according to the features of their boundary layers, with the taxonomy of local climate zones for urban temperature studies (LCZ) proposed by Stewart and Oke [1].

The relationship between CWTs and air temperatures was analysed by representing the distribution of the seasonal daily thermal range (DTR) for the five weather stations classified in terms of LCZs, distinguishing weather regimes as either cyclonic or anticyclonic (CWT 2, 5 and 10 and CWT 8, 11 and 16, respectively) during the four Seasons (winter = December–February; spring = March–May; summer = June–August; autumn = September–November). The analysis was limited to the three cyclonic (2, 5 and 10) and three anticyclonic (8, 11 and 16) CWTs because they give rise to more easily discernible DTR distributions. This choice was dictated by the need to have types capable of providing sensitive dynamic and thermal effects in the Milan area.

Specifically, the Genoa low (CWT 2) is a peculiar pattern related to the Gulf of Genoa, which is the main cyclogenetic zone of the Mediterranean, whereas troughs from the northwest (CWT 5) and from the northeast (CWT 10) give rise to strong advection of Polar maritime and Arctic air, respectively. Moreover, anticyclonic CVTs 8, 11 and 16 effectively give rise to advection of peculiar stable air masses (subtropical continental for CVT 8, subtropical maritime for CVT 11 and Arctic for CVT 16).

Statistical analysis of the significance of differences was performed on all the measurements by means of a mixed-model ANOVA, considering the groups seasons, LCZs and weather regimes, followed by a Sidak post hoc test for mean comparison [36].

2.2. A Case Study under Anticyclonic Conditions

In order to analyse the effects of a large park on the UHI of Milan under anticyclonic conditions, a 24-h monitoring campaign was carried out on 23 July 2015 in the presence of a strong summer dynamic anticyclone (CWT 11). Two bicycle transects (Figure 2 and Table 2) were defined to monitor the air temperature in the area of Parco Nord Milano and in the neighbouring urban areas. The sampling points along the transects were classified with local climate zones [1].

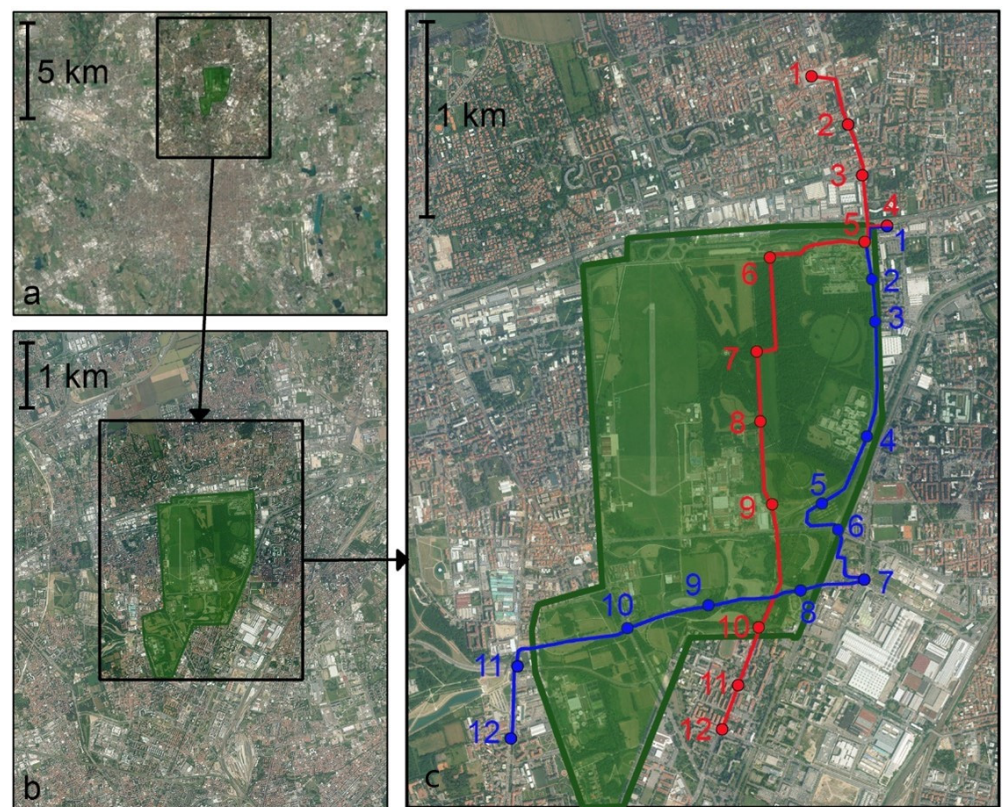


Figure 2. (a,b) Location of Parco Nord in the context of the urban area of Milan. (c) Transects of the bike monitoring activity (transect 1—red line, transect 2—blue line).

Table 2. Transect check points with LCZ classification.

Transect 1			Transect 2		
	Name	LCZ		Name	LCZ
1	Cinisello B. Central square	2	1	Hotel parking lot	2
2	Libertà St.	2	2	Gorki St./Canzio St. intersection	9
3	Martinelli St. roundabout	2	3	Gorki St./Ferri St. intersection	9
4	Hotel parking lot	2	4	School 2	9
5	Turollo St./Gorki St. intersection	9	5	Clerici St. parking lot	B
6	Park—north entrance	B	6	Clerici St./Testi St. intersection	B
7	Park—Cypress boulevard 1	B	7	Mall intersection	B
8	Park—Cypress boulevard 2	B	8	Bridge—east side	B
9	Park—ascent to footbridge	B	9	Park—velodrome	B
10	Suzzani St.	2	10	Park—Finanzieri d'Italia St.	9
11	Suzzani St./Arezzo St. intersection	2	11	Veneto St./Regno Italico St. intersection	9
12	Suzzani St./Ponale St. intersection	2	12	Ornato St./Guido da Velate St. intersection	2

Transect 1 (red line in Figure 2) traverses along the north–south direction. It begins in the centre of the municipality of Cinisello Balsamo, crosses the middle of the park and reaches the northern urban area of Milan at Suzzani Street.

Transect 2 (blue line in Figure 2), start from the area near Cosmo Hotel in Cinisello Balsamo on the northeastern side of the park, runs along the eastern side of the park and crosses the southern side of the park in the east–west direction and reaching the northern urban area of Milan at Ornato Street.

High-resolution A-class PT100 thermometers with a very short response time, together with high-sampling-rate data loggers (10 s), were mounted on the backs of bicycles.

The transects were ridden by bike every two hours for a 24 h period. Air temperature was continuously monitored. At every sampling point, bikes stopped for 30 s to obtain a reliable measurement of temperature.

Statistical analysis was performed on all measurements of air temperature along the transects by means of a mixed-model ANOVA, considering the groups LCZs and hours, followed by Sidak post hoc test for mean comparison [36].

3. Results and Discussion

3.1. Analysis of the Weather Types and Their Effects on City Thermal Behaviour

Table 3 shows the number of CWTs per year during the 2002–2015 period.

Table 3. CWT monthly classification from 2002 to 2015.

	2002	2003	2004	2005	2006	2007	2008	2009	2010	2011	2012	2013	2014	2015	AVG	St. Dev
1	79	46	33	31	32	42	41	27	46	36	43	66	70	31	44.5	16.1
2	29	12	39	47	21	28	31	60	76	48	42	82	59	72	46.1	21.4
3	3	2	2	5	0	0	0	0	0	2	5	5	0	6	2.1	2.3
4	52	59	48	51	59	38	36	43	39	63	46	31	31	51	46.2	10.3
5	15	10	18	18	11	12	18	27	17	14	14	19	34	19	17.6	6.4
6	9	6	26	14	14	23	6	24	10	25	19	7	4	5	13.7	8.2
7	10	4	14	21	9	25	8	10	13	15	27	13	21	18	14.9	6.7
8	29	57	34	38	26	14	31	26	23	33	43	44	35	39	33.7	10.5
9	40	41	29	13	24	38	42	15	13	24	20	37	66	47	32.1	15.1
10	31	50	42	70	67	57	94	68	67	18	41	30	13	16	47.4	24.3
11	23	28	31	23	46	31	9	25	13	43	35	21	11	47	27.6	12.3
12	31	17	18	12	17	11	15	7	11	8	16	0	10	2	12.5	7.6
13	1	12	2	4	11	12	19	5	4	1	3	0	3	2	5.6	5.6
14	3	4	4	0	0	4	1	1	2	0	2	3	0	0	1.7	1.6
15	7	15	0	0	8	4	0	3	3	6	3	3	4	8	4.6	4.1
16	3	2	1	1	3	15	2	3	0	5	3	2	3	2	3.2	3.6
17	0	0	25	17	17	11	13	21	28	24	4	2	1	0	11.6	10.4

Figure 3 shows the distribution of the seasonal daily thermal range (DTR) for the five weather stations. Figures on the left there are the distributions related to cyclonic CWTs 2, 5 and 10, whereas those on the right are the distributions related to anticyclonic CWTs 8, 11 and 16.

Table 3 shows the number of samples used (2002–2015). Based on visual analysis, in all four seasons, it is possible to clearly distinguish the behaviour of the two LCZ2 stations (Milan Brera and Milan Marche) compared to the LCZB stations (Parco Nord Milano and Montanaso Lombardo), whereas the LCZ9 station (Milan Zavattari) exhibits intermediate behaviour. The Parco Nord Milano station exhibits behaviour very similar to that of the rural station in Montanaso Lombardo; the differences between these two stations can be attributed to the exchange of air in the Parco Nord Milano area with the surrounding urban areas (breeze effects).

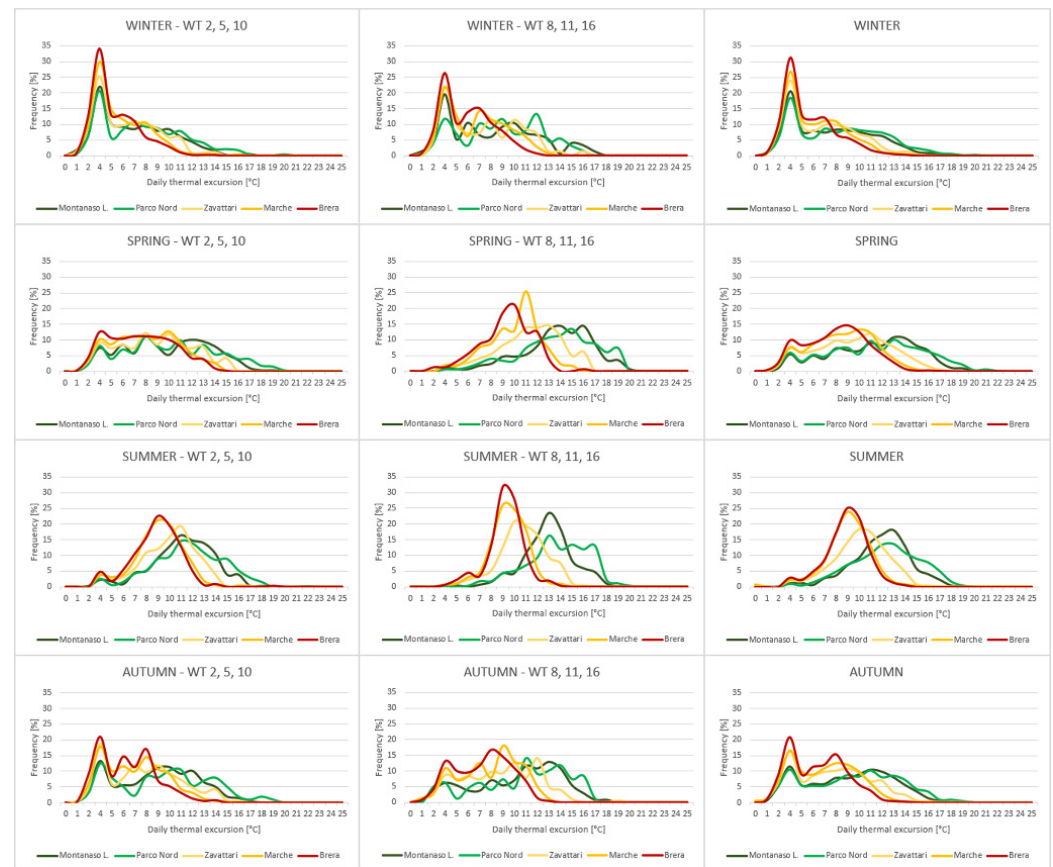


Figure 3. Distribution of the seasonal daily thermal range (DTR) for the five weather stations.

Anticyclonic CWTs show the effects of different LCZs more clearly than those of cyclonic CWTs, with noise resulting from the following factors:

- Enhanced cloud coverage for cyclonic CWTs with damping of the long-wave emission and diurnal radiative force;
- Anticyclonic days are affected by breezes, whereas during cyclonic CWTs, breezes are substituted by synoptic circulation.

The summer season shows the most relevant difference between the LCZs in terms of DTR behaviour, which can be accounted for by the increased solar radiative force enhancing all the terms of the surface energy balance.

Figure 3 highlights the peculiarities of the urban environment compared to the rural environment in terms of the frequencies of the various DTR values. In particular, whereas the rural area has higher DTR frequency peaks in the case of anticyclonic types 8, 11 and 16 with respect to the city, the weather types do not affect the peak, which is located at 9–10 °C for the summer and at 4 °C for the winter. This shows an overall stabilizing effect of the city, giving rise to an “urban signature” peculiar to specific cities linked to the shape of the urban LCZs and deriving cooling by radiation, as well as by mechanical and thermal mixing.

In terms of weather types, among a total number 12,190 DTR measurements from the five weather stations, 4460 measurements fell under cyclonic conditions and 7730 under anticyclonic conditions. In terms of LCZs, the series accounted for 4876 measurements for LCZB (Parco Nord and Montanaso L.), 2348 for LCZ9 (Zavattari) and 4876 for LCZ2 (Marche and Brera). In terms of seasons, the measurements were divided as follows: 2660 in winter, 2810 in spring, 3435 in summer and 3825 in autumn.

For statistical analysis, data were gathered considering:

- LCZ (2, 9 or B);
- Season (winter, spring, summer or autumn); and
- CWT group (cyclonic or anticyclonic)

Statistical analysis of all the measurements by means of a mixed-model ANOVA showed a significant triple interaction among seasons, LCZs and CWT regimes. The results of the Sidak post hoc test for mean comparison are shown in Tables 4–6.

Table 4. Significance of the difference among seasons for each LCZ and CWT. Average values (°C) are shown. Letters a, b, c, d represent significant differences among groups.

LCZ	CWT Group	Season			
		Winter	Spring	Summer	Autumn
2	Anticyclonic	5.40 a	8.84 b	8.77 b	6.64 c
2	Cyclonic	4.62 a	7.07 b	8.40 c	5.79 d
9	Anticyclonic	6.54 a	10.13 b	9.60 b	7.75 c
9	Cyclonic	5.38 a	7.89 b	9.04 c	6.75 d
B	Anticyclonic	8.02 a	13.28 b	12.80 b	9.98 c
B	Cyclonic	6.72 a	9.51 b	10.93 c	8.59 d

Table 5. Significance of DTR variation among CWT groups for each Season and each LCZ. Average values [°C] are shown. Letters a, b represent significant differences among groups.

Season	LCZ	CWT Group	
		Cyclonic	Anticyclonic
Winter	2	4.62 a	5.40 a
	9	5.38 a	6.54 b
	B	6.72 a	8.02 b
Spring	2	7.07 a	8.84 b
	9	7.89 a	10.13 b
	B	9.51 a	13.28 b
Summer	2	8.40 a	8.77 a
	9	9.04 a	9.60 a
	B	10.93 a	12.80 b
Autumn	2	5.79 a	6.64 a
	9	6.75 a	7.75 b
	B	8.59 a	9.98 b

Table 6. Significance of DTR variation among LCZ groups for each Season and each CWT. Average values [°C] are shown. Letters a, b represent significant differences among groups.

Scheme	CWT Group	LCZ		
		2	9	B
Winter	Anticyclonic	5.40 a	6.54 a	8.02 a
	Cyclonic	4.62 a	5.38 a	6.72 a
Spring	Anticyclonic	8.84 a	10.13 ab	13.28 b
	Cyclonic	7.07 a	7.89 a	9.51 a
Summer	Anticyclonic	8.77 a	9.60 ab	12.80 b
	Cyclonic	8.40 a	9.04 a	10.93 a
Autumn	Anticyclonic	6.64 a	7.75 a	9.98 a
	Cyclonic	5.79 a	6.75 a	8.59 a

DTR values significantly differ from season to season (Table 4), independent of LCZ type during anticyclonic types. A similar behaviour is observed during cyclonic types, with the exception of spring and summer, which do not show significant differences.

Considering the CWT groups (Table 4), significant differences are shown in autumn by LCZ 9 and B; in spring by LCZ 2, 9 and B; in summer by LCZ B; and in winter by LCZ 9. Finally, focusing on LCZs, during anticyclonic CWTs, in spring and summer, a transition occurs from LCZ B to 9 to 2.

Under cyclonic CWTs, for all the LCZs, the DTR significantly differs across the four seasons. During the summer, cyclonic CWTs are associated with convective cloudiness, which develops in the presence of higher DTRs than those that occur in spring and autumn, when cloudiness is more often of a stratified type and, resulting in lower DTRs. The poor winter radiative force accounts for the lower DTR compared to the other seasons.

Under anticyclonic CWTs, spring and summer are homogeneous with each other in terms of DTR but differ significantly compared to autumn and winter. We do not have an explanation for this phenomenon that is observed in the data.

Table 5 shows that in the LCZB environments, the cyclonic CWTs fully perform their action on the surface energy balance in all seasons, giving rise to significant differences in DTRs compared to anticyclonic CWTs. On the contrary, the zone with the highest UHI (LCZ2) shows a non-significant difference in terms of DTR between cyclonic and anticyclonic types in winter, summer and autumn, which is observed for LCZ9 for the summer only. These phenomena can be attributed to the stabilizing effect induced by the UHI with respect to the perturbations of the surface energy balance determined by cyclonic CWTs.

A comparison among LCZs (Table 6) shows that the only seasons in which LCZs significantly affect the DTR are spring and summer under anticyclonic conditions, when the high solar force during the day is counterbalanced by night-time cooling and enhanced by the increased sky view factor in LCZB.

The influence of CVTs on ground weather conditions in urban areas highlighted in this work was also observed by Guo et al. [27], who analysed the modulation of DTR by various synoptic weather patterns in the Yangtze River Delta region (YRDUA) in eastern China, showing the effects on subareas within the studied region.

The effect of CVT on UHI is obviously modulated by the peculiarities of the climate of the studied area, in terms of types of weather, latitude (radiative forcing) and distribution of cloud cover and rain (linked to the types of weather). From this point of view, it is fundamental to remember the peculiar characteristics of the Po Valley area located downstream of the Alpine chain, with an average height of 3000 m a.s.l. This makes the boundary layer particularly stable during anticyclonic phases, allowing, for example, the accumulation of large amounts of moisture in the air mass, which are conducive to triggering summer thunderstorms.

3.2. Transects

Figures 4 and 5 show the air temperatures monitored along transects 1 and 2. The green colour represents the areas inside the park (LCZ B), whereas the city points (LCZ9 and LCZ2) are represented by dark and light grey, respectively. The thermal difference between the various LCZs reaches its maximum during night conditions (hh 6 p.m., 12 a.m., 2 a.m. and 4 a.m.). On the contrary, the daytime vertical mixing driven by solar radiation (hh 10 a.m., 12 p.m., 4 p.m. and 6 p.m.) determines a homogenization of different LCZs, which extends to the evening and the first night (20, 22).

Statistical analysis of all the measurements of the transect by means of a mixed-model ANOVA showed a significant interaction between hour and LCZs. The results of the Sidak post hoc test for mean comparison are shown in Table 7.

Figure 6 shows the statistics of all the temperature samplings gathered in the same LCZ for each hour. Statistical analysis (Table 7) confirmed the significance of the difference between LCZB and LCZ2 during the night hours.

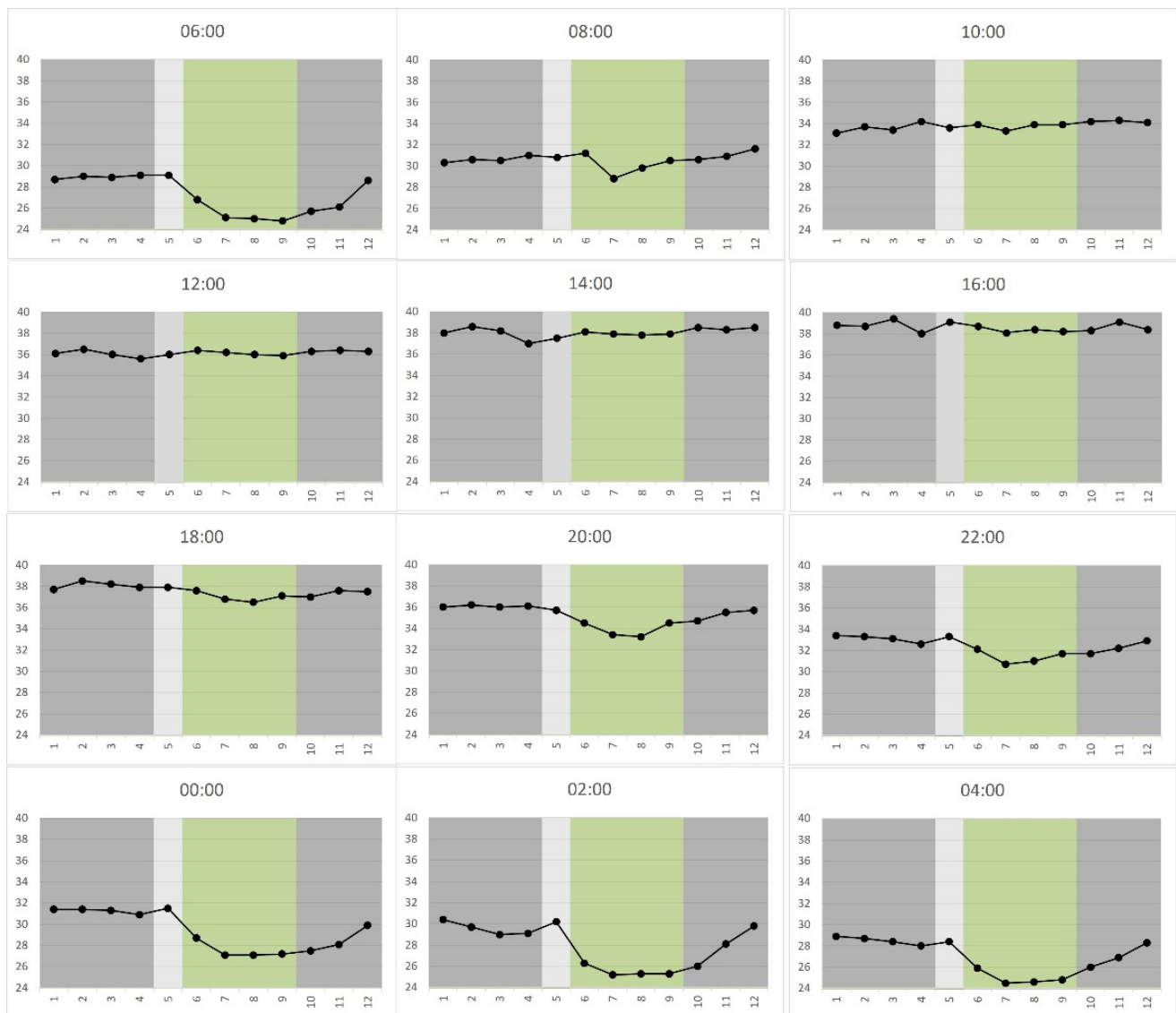


Figure 4. Transect 1—charts of single-lap measurements. LCZs are represented with different background colours: 2—dark grey; 9—light grey; B—green; Y axis reports air temperatures in °C.

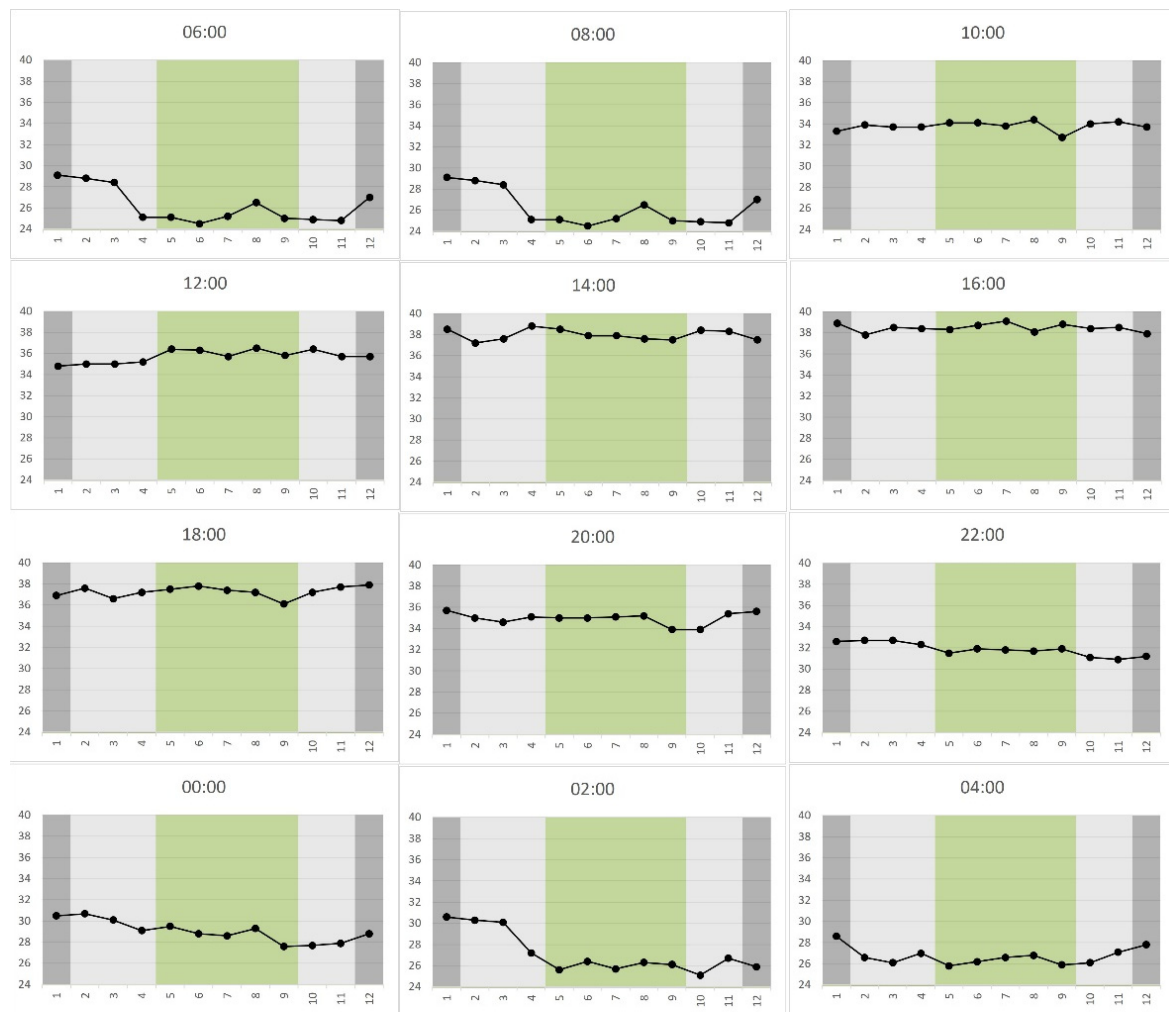


Figure 5. Transect 2—charts of single-lap measurements. LCZs are represented with different background colours: 2—dark grey; 9—light grey; B—green; Y axis reports air temperatures in °C.

Table 7. Significance of the difference among LCZs for each hour along the transects measurements. Average values [°C] are shown. Letters a, b represent significant differences among groups.

Hour	LCZ2	LCZ9	LCZB
2	28.6 a	28.3 a	25.8 b
4	27.9 a	26.9 a	25.7 b
6	27.9 a	26.9 a	25.3 b
8	30.9 a	30.6 a	30.3 a
10	33.9 a	33.8 a	33.8 a
12	36.1 a	36 a	35.5 a
14	38.1 a	38 a	37.9 a
16	38.6 a	38.5 a	38.5 a
18	37.7 a	37.4 a	37.1 a
20	35.7 a	35 ab	34.4 b
22	32.5 a	32.2 a	31.6 a
24	29.9 a	29.5 a	28.2 b

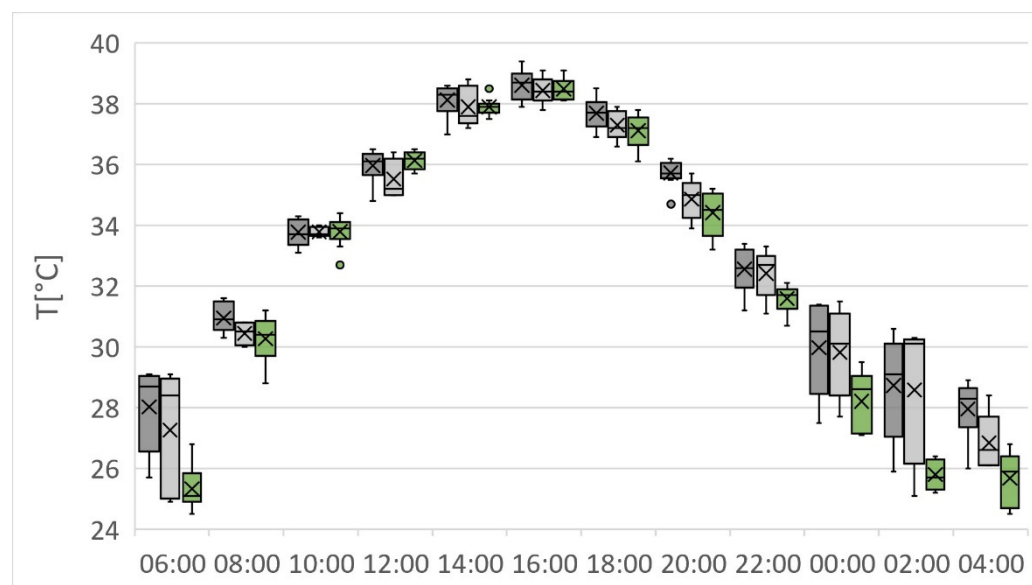


Figure 6. Hourly statistics of LCZ temperature, considering all the sampling points of the two transects; Y axis reports air temperatures in °C. For each value X represents the average, the horizontal line is the median, the box extends from upper to lower quartile. The whiskers (vertical lines outside the box) represent data variability outside the upper and lower quartiles. Points outside the whisker line represent the outlier data.

However, positive effects of the park should not be exclusively sought in the analysis of the thermal regime, as shown by these results, as other factors act in determining their effectiveness in terms of mitigation of urban effects. Among these, breeze circuits of green areas (which are not limited by the barriers constituted by buildings) and shading effects caused by treetops and structures play important roles [37].

The city has a strong impact on the trend of the DTR, with a lower sensitivity to the types of weather than rural environments.

Analysis of the data in Table 7 shows that during the day (from 8 a.m. to 8 p.m.) LCZ2, LCZ9 and LCZB exhibit homogeneous thermal behaviour due to the sensitive vertical mixing of the air mass, which is induced by intense sunshine and that minimizes differences in the temperature of the air above non-homogeneous surfaces [38]. On the contrary, in the evening and at night, the UHI effect quickly takes hold, resulting in reduced cooling in LCZ2 and LCZ9, which therefore present with a significant difference in behaviour compared to LCZB. This effect is a consequence of the fact that in the urban environment, the loss of radiation toward space is slowed by the reduced sky vision factor. Furthermore, the absence of significant differences between LCZB, LCZ2 and LCZ9 at 10 pm could have a circulatory origin (breezes).

Despite its limitation (only one day was considered), the case study of the transect helped us to clarify the role of the city in the occurrence of anticyclonic days, which are associated with summer heatwaves with peculiar conditions (high solar radiation, clear sky, vertical compression heating effects and very weak or calm wind). Our results highlight that during this specific CWT, the park effectively mitigates the UHI but that this effect only takes place within the park itself and vanishes completely within a short distance beyond the boundary of the park itself.

This evaluation is preliminary and refers to a specific CWT. A more exhaustive evaluation should be carried out with reference to a much larger number of cases, which is possible, for example, with the use of remote sensing [39].

4. Conclusions

In order to understand the behaviour of the UHI of the metropolitan city of Milan, a daily analysis for the period 2002–2015 was carried out, highlighting the effects of some

CWTs (cyclonic or anticyclonic) on the DTR in three LCZs (2, 9 and B) and for the four seasons. Moreover, the thermal effects of these three LCZs were analysed by means of a transect analysis carried out for an anticyclonic summer CWT.

Analysis of the effect of cyclonic and anticyclonic CWTs on the frequency distribution of DTR was performed for five weather stations characterized by different features, as represented by the Stewart and Oke LCZs. Most urban areas (LCZ2) exhibit a peculiar signature, especially in winter and summer (the two extreme seasons in terms of radiative force), generating a modal class (4 °C in winter and 9 °C in summer) that stabilizes and minimizes the DTR in comparison to less dense sectors of the city (LCZs 9 and B).

Temperature transects of the urban park Parco Nord performed by bicycle during a day of anticyclonic summer weather (CWT 11) highlighted the homogenization effect on temperatures induced by the thermal turbulence triggered by intense sunshine during daytime. As a consequence, the variation in DTR of the different LCZs is mostly determined by night-time temperature, as the park enables cooling.

Author Contributions: G.S.: conceptualization, methodology, formal analysis, investigation, writing and revising and funding acquisition; G.C. (Giuseppe Colangelo): conceptualization, data collection, formal analysis, investigation, writing and revising; L.M.: data collection, formal analysis, investigation, writing and revising; S.G.P.: data collection, formal analysis, investigation, writing and revising; G.C. (Gabriele Cola): conceptualization, data collection, formal analysis, investigation, writing, revising and supervision. All authors have read and agreed to the published version of the manuscript.

Funding: This work was funded by the project “Establishing Urban FORest based solutions In Changing Cities (EUFORICC)” and financially supported by the Ministry of Education, University and Research (MIUR) of Italy (PRIN 20173RRN2S).

Informed Consent Statement: Not applicable.

Conflicts of Interest: The authors declare that the research was conducted in the absence of any commercial or financial relationships that could be construed as a potential conflict of interest.

Abbreviations

The following abbreviations are used in this manuscript:

CWT	anticyclonic circulation weather types
DTR	daily thermal range
LCZ	local climate zones for urban temperature studies
PNM	Parco Nord Milan
UHI	urban heat island

References

1. Stewart, I.D.; Oke, T.R. Local climate zones for urban temperature studies. *Bull. Am. Meteorol. Soc.* **2012**, *93*, 1879–1900. [\[CrossRef\]](#)
2. Varquez, A.C.G.; Kanda, M. Global urban climatology: A meta-analysis of air temperature trends (1960–2009). *Npj Clim. Atmos. Sci.* **2018**, *1*, 32. [\[CrossRef\]](#)
3. Oke, T.R. The energetic basis of the urban heat island. *Q. J. R. Meteorol. Soc.* **1982**, *108*, 1–24. [\[CrossRef\]](#)
4. Oke, T.R. *Boundary Layer Climates*; Taylor & Francis: Abingdon, UK, 2002; p. 464.
5. Mariani, L.; Parisi, S.; Cola, G.; Laforteza, R.; Colangelo, G.; Sanesi, G. Climatological analysis of the mitigating effect of vegetation on the urban heat island of Milan, Italy. *Sci. Total Environ.* **2016**, *569*, 762–773. [\[CrossRef\]](#)
6. Barry, R.G.; Carleton, A.M. *Synoptic and Dynamic Climatology*; Routledge: London, UK; New York, NY, USA, 2011; p. 620.
7. Weusthoff, T. Weather Type Classification at MeteoSwiss—Introduction of new automatic classifications schemes. *Arb.-Ber. Der MeteoSchweiz* **2011**, *235*, 46.
8. James, P.M. An objective classification method for Hess and Brezowsky Grosswetterlagen over Europe. *Theor. Appl. Clim.* **2007**, *88*, 17–42. [\[CrossRef\]](#)
9. Spellman, G. An assessment of the Jenkinson and Collinson synoptic classification to a continental mid-latitude location. *Arch. Meteorol. Geophys. Bioclimatol. Ser. B* **2016**, *128*, 731–744. [\[CrossRef\]](#)
10. Michaelides, S.C.; Iassidou, F.L.; Schizas, C.N., Synoptic Classification and Establishment of Analogues with Artificial Neural Networks. *Pure Appl. Geophys.* **2007**, *164*, 1347–1364. [\[CrossRef\]](#)

11. Chattopadhyay, A.; Hassanzadeh, P.; Pasha, S. Predicting clustered weather patterns: A test case for applications of convolutional neural networks to spatio-temporal climate data. *Sci. Rep.* **2020**, *10*, 142–149. [\[CrossRef\]](#)
12. Ramos, A.M.; Barriopedro, D.; Dutra, E. Circulation weather types as a tool in atmospheric, climate, and environmental research. *Front. Environ. Sci.* **2015**, *3*, 44. [\[CrossRef\]](#)
13. Gilabert, J.; Llasat, M.C. Circulation weather types associated with extreme flood events in Northwestern Mediterranean. *Int. J. Clim.* **2018**, *38*, 1864–1876. [\[CrossRef\]](#)
14. Maheras, P.; Tolika, K.; Anagnostopoulou, C.; Makra, L.; Szpirosz, K.; Károssy, C. Relationship between mean and extreme precipitation and circulation types over Hungary. *Int. J. Clim.* **2018**, *38*, 4518–4532. [\[CrossRef\]](#)
15. Putniković, S.; Tošić, I.; Đurđević, V. Circulation weather types and their influence on precipitation in Serbia. *Arch. Meteorol. Geophys. Bioclimatol. Ser. B* **2016**, *128*, 649–662. [\[CrossRef\]](#)
16. Bissolli, P.; Grieser, J.; Dotzek, N.; Welsch, M. Tornadoes in Germany 1950–2003 and their relation to particular weather conditions. *Glob. Planet. Chang.* **2007**, *57*, 124–138. [\[CrossRef\]](#)
17. Gayà, M. Tornadoes and severe storms in Spain. *Atmos. Res.* **2011**, *100*, 334–343. [\[CrossRef\]](#)
18. Demuzere, M.; van Lipzig, N.P.M. A new method to estimate air-quality levels using a synoptic-regression approach. Part I: Present-day O₃ and PM₁₀ analysis. *Atmos. Environ.* **2010**, *44*, 1341–1355. [\[CrossRef\]](#)
19. Demuzere, M.; Kassomenos, P.; Philipp, A. The COST733 circulation type classification software: An example for surface ozone concentrations in Central Europe. *Arch. Meteorol. Geophys. Bioclimatol. Ser. B* **2010**, *105*, 143–166. [\[CrossRef\]](#)
20. Morris, C.J.G.; Simmonds, I. Associations between varying magnitudes of the urban heat island and the synoptic climatology in Melbourne, Australia. *Int. J. Climatol.* **2000**, *20*, 1931–1954. [\[CrossRef\]](#)
21. Mihalakakou, G.; Flocas, H.A.; Santamouris, M.; Helmis, C.G. Application of Neural Networks to the Simulation of the Heat Island over Athens, Greece, Using Synoptic Types as a Predictor. *J. Appl. Meteorol.* **2002**, *41*, 519–527. [\[CrossRef\]](#)
22. Kassomenos, P.A.; Katsoulis, B.D. Mesoscale and macroscale aspects of the morning Urban Heat Island around Athens, Greece. *Arch. Meteorol. Geophys. Bioclimatol. Ser. B* **2006**, *94*, 209–218. [\[CrossRef\]](#)
23. Półrolniczak, M.; Kolendowicz, L.; Majkowska, A.; Czernecki, B. The influence of atmospheric circulation on the intensity of urban heat island and urban cold island in Poznań, Poland. *Arch. Meteorol. Geophys. Bioclimatol. Ser. B* **2015**, *127*, 611–625. [\[CrossRef\]](#)
24. Halios, C.H.; Flocas, H.A.; Helmis, C.G.; Asimakopoulou, D.N.; Mouschouras, P.G. Observations of Local Meteorological Variability under Large-Scale Circulation Patterns over Athens, Greece. *Atmosphere* **2018**, *9*, 25. [\[CrossRef\]](#)
25. Katavoutas, G.; Flocas, H.A. Universal thermal climate index (UTCI) and synoptic circulation patterns over the metropolitan city of Athens, Greece. *Glob. NEST J.* **2018**, *20*, 477–487.
26. Anjos, M.; Crespo Targino, A.; Krecl, P.; Yoshikazu Oukawa, G.; Favaro Braga, R. Analysis of the urban heat island under different synoptic patterns using local climate zones. *Build. Environ.* **2020**, *185*, 107268. [\[CrossRef\]](#)
27. Guo, M.; Zhang, M.; Wang, H.; Wang, L.; Liu, S.; Zong, L.; Zhang, Y.; Li, Y. Dual effects of synoptic weather patterns and urbanization on summer diurnal temperature range in an urban agglomeration of East China. *Front. Environ. Sci.* **2021**, *9*, 672295. [\[CrossRef\]](#)
28. Stull, R.B. *An Introduction to Boundary Layer Meteorology*; Kluwer Academic Publishers: Dordrecht, The Netherlands, 1997; p. 670.
29. Munn, R.E. *Descriptive Micrometeorology*; Academic Press: New York, NY, USA; London, UK, 1966; p. 245.
30. Koeppen, W.; Geiger, R. *Handbuch der Klimatologie*; Verlag von Gebrüder Borntraege: Berlin, Germany, 1936.
31. Sanesi, G.; Laforteza, R.; Marziliano, P.A.; Ragazzi, A.; Mariani, L. Assessing the current status of urban forest resources in the context of Parco Nord, Milan, Italy. *Landsc. Ecol. Eng.* **2007**, *3*, 187–198. [\[CrossRef\]](#)
32. Parisi S, Cola G, Colangelo G, Laforteza R, Mariani L, Sanesi G. Meteorological effects of the urban forest Parco Nord (Milan, Italy). *Urban Clim. News* **2018**, *48*, 16–19.
33. Giuliacci, M. *Climatologia Storica e Dinamica Della Valpadana*; CNR: Milano, Italy, 1985; p. 222.
34. NOAA—National Oceanic and Atmospheric Administration—U.S. 2022. Available online: <https://psl.noaa.gov/cgi-bin/data/composites/plot20thc.day.v2.pl> (accessed on 10 May 2022).
35. Lupo, A.R.; Smith, P.J. Climatological features of blocking anticyclones in the Northern Hemisphere. *Artic. Tellus* **1995**, *47*, 439–456. [\[CrossRef\]](#)
36. Šidák, Z.K. Rectangular Confidence Regions for the Means of Multivariate Normal Distributions. *J. Am. Stat. Assoc.* **1967**, *62*, 626–633.
37. Marziliano, P.A.; Laforteza, R.; Colangelo, G.; Davies, C.; Sanesi, G. Structural diversity and height growth models in urban forest plantations: A case-study in northern Italy. *Urban For. Urban Green.* **2013**, *12*, 246–254. [\[CrossRef\]](#)
38. Fabrizi, R.; Bonafoni, S.; Biondi, R. Satellite and Ground-Based Sensors for the Urban Heat Island Analysis in the City of Rome. *Remote Sens.* **2010**, *2*, 1400–1415. [\[CrossRef\]](#)
39. Yao, X.; Yu, K.; Zeng, X.; Lin, Y.; Ye, B.; Shen, X.; Liu, J. How can urban parks be planned to mitigate urban heat island effect in “Furnace cities”? An accumulation perspective. *J. Clean. Prod.* **2021**, *330*, 129852. [\[CrossRef\]](#)